Dynamic Modelling and Vibration Control of a Turbomolecular Pump with Magnetic Bearings in the Presence of Blade Flexibility

Alysson Bruno Barbosa Moreira, Fabrice Thouverez

Proceedings of ASME Turbo Expo 2019: Turbomachinery Technical Conference and Exposition
GT2019
June 17-21, 2019, Phoenix, Arizona, USA

GT2019-90990

INFLUENCE OF BLADE FLEXIBILITY ON THE DYNAMIC RESPONSE SIMULATION OF A TURBOMOLECULAR PUMP ON MAGNETIC BEARINGS

Alysson Bruno Barbosa Moreira
Laboratoire de Tribologie et
Dynamique des Systèmes, UMR-CNRS 5513
École Centrale de Lyon
69134 Écully Cedex, France
Email: bruno.moreira@doctorant.ec-lyon.fr

Fabrice Thouverez *
Laboratoire de Tribologie et
Dynamique des Systèmes, UMR-CNRS 5513
École Centrale de Lyon
69134 Écully Cedex, France
Email: fabrice.thouverez@ec-lyon.fr

ABSTRACT

This paper proposes the simulation of a complete mechanical model of a turbomolecular pump rotor, including rotor and blades flexibility, suspended by controlled active magnetic bearings. The mechanical model is composed of an eight stage blisk, attached to a shaft. Magnetic forces are linearized by first order Taylor expansion around a given point. Including blades and rotor flexibility makes the mechanical system asymmetric, so the equations of motion for the coupled system have periodic terms. A modal controller was designed to control rigid body modes, since the number of sensors is limited and no state observer is implemented. PID controllers are used for low frequency modes combined with second order filters to damp high frequency modes. First of all, stability analysis was carried out for the axisymmetric case. Secondly, blades flexibility was included. Forced response of the whole system to an impulsive force was studied. Divergent responses for the system in rotation were obtained as a second order filter pole possibly interacts with blades modes. Taking second order filters off the control loop allowed the system to be stable. These results show that the analysis method developed here is efficient to evaluate the performance of a controller in closed loop with the complete flexible system. This method may be used in industrial design processes as computation times for the complete system are very short.

*Address all correspondence to this author.

NOMENCLATURE

AMB Active Magnetic Bearing
$\mathbf{D}$ Global damping matrix (rotating frame)
$\mathbf{F}_a$ Magnetic forces vector
F_{mag} Magnetic force
$\mathbf{G}(\Omega)$ Global gyroscopic matrix (rotating frame)
$\mathbf{K}$ Global stiffness matrix (rotating frame)
$\mathbf{K}_i$ Magnetic bearing electric stiffness matrix
$\mathbf{K}_{mag}$ Negative stiffness matrix in Rayleigh-Ritz basis
$\mathbf{K}_s$ Magnetic bearing negative stiffness matrix
$\mathbf{M}$ Mass matrix (rotating frame)
$\mathbf{N}(\Omega^2)$ Spin softening matrix (rotating frame)
R rotating frame
$\mathbf{R}(\Omega t)$ Rotation matrix
W_{F_a} Work of magnetic forces
$\boldsymbol{f}$ Generalized forces (rotating frame)
i_a Vector of control currents
$\boldsymbol{q}$ Generalized coordinates (rotating frame)
x_p Displacement of the rotors at magnetic bearings position
x^*_{ref} Arbitrary normalization displacement. Used for all graphical representations
x_s Displacement of the rotors at sensors positions
Ω Spin speed
Ω_n Nominal spin speed
Θ_s Sensors transformation matrix from generalized to physical coordinates

Θ_p Actuators transformation matrix from generalized to physical coordinates

ω Frequency

ω_{ref} Arbitrary normalization frequency. Used for all graphical representations

$\bullet^*$ Variable described in the stationary frame. When variables are also described in rotating frame, they are not noted with asterisk

INTRODUCTION

Turbomolecular pumps generate high levels of vacuum via particle collision principle: blades rotating at high speed transfers velocity component to the molecule pushing it out the vacuum chamber. Such pumps are composed of a multistage blisk, attached to a rotating shaft, supported by active magnetic bearings (AMB). The advantages of this kind of bearings are their high reliability, contamination free operation as no lubrication is needed and low levels of vibration at very high rotation speeds [1, 2].

Since magnetic forces are inversely proportional to the square of the distance between shaft and bearings, AMB realizations are naturally unstable. Furthermore, the relation between current and magnetic forces is nonlinear [3]. For those reasons, AMB supporting turbomolecular pumps are actively controlled. Additionally, these controllers can be used to damp pump vibrations.

Dynamic response of rotors suspended by actively controlled AMB has been studied by many researchers, the majority of them aiming to design a control strategy or to evaluate its performance. Most of the models used to simulate rotor structural dynamics can be divided in two levels of complexity: those who consider rotor as a rigid body and develop their control law based only on this phenomenology and those who take into account the flexibility of the shaft (see works [3–8]). Very few works simulate rotating blades flexibility in a system coupled with a controller acting in the stationary frame, like magnetic bearings. The difficulties that arise from this approach are due to the fact that since the rotor is no longer axisymmetric, its equations of motion in the stationary frame, where control forces actuate, are time periodic [9].

In a previous work [10], authors have presented experimental data of a functioning pump which demonstrates that blades dynamics may be a significant factor in controlled closed loop analysis. At some operating conditions, blades response has significant amplitude, indicating that they are excited by the controller. Such interaction may be of great interest for manufacturers, as it can reduce the machine's lifetime or lead to unpredicted structural failures.

The investigation of Christensen *et al* [11] is one example of studies of rotating flexible bladed rotor supported by actively controlled bearings. In this encouraging work, controller is designed considering a rigid rotor on actively controlled linear bearings. To the rotor is attached to a flexible bladed disk. Only planar motions are considered (gyroscopy is neglected). Control design was carried out using a periodic modal transformation initially proposed by [12]. In this respect, some works propose methods for the stability analysis of linear time periodic variant systems based on periodic modal analysis, like [13]. Terms as "pseudo-modes" and "pseudo-natural frequencies" are introduced [14].

It has to be noted that such methods are not yet applied to sophisticated multistage rotor-blisk systems such as turbomolecular pumps. Hence, for industrial applications one may prefer control design methods that consider only shaft dynamics. Nevertheless, simulating the response of the complete system is time and money saving, as it allows to assess the interaction between rotating mechanical parts (including blades flexible motion) and controller before manufacturing and tests.

In this context, the aim of this work is to propose the forced response simulation of the complete turbomolecular pump rotor, including blades flexibility, coupled with a stabilizing controller for the axisymmetric system. Such simulations are able to describe the closed loop full system behavior, allowing the interactions between the control law and all the structural components to be studied.

The implemented control law is designed based on a rigid body model of the pump. A modal controller including rigid body modes is proposed. With the above simulations, one can evaluate the effects of a rigid body based controller on the rotor and blades flexibility. This avoids the implementation of sophisticated methods for periodic time dependent systems stability analysis.

This paper is organized as follows: first the mechanical part of the rotor and positioning of sensor and actuators are described, the equations of motions derived in a previous work are recalled. Then, magnetic forces linearized equations are derived in function of rotor displacements and control currents. Coupling of magnetic forces and mechanical equations of motion is proposed in the following section. Thereafter, the control law used to stabilize the axisymmetric system is described and stability analysis results for the rotating system are presented. Finally, forced response to an impulse excitation of the complete flexible bladed rotating system is presented and the results are discussed.

DESCRIPTION OF THE ROTOR'S MODEL

The model that describes the pump's dynamic behavior is presented in Fig. 1. It is composed of a flexible shaft, on which a bladed disk is attached with a flexible element (k_m). The disk is considered rigid and axisymmetric, only its mass and moments of inertia are included in the model. Eight stages of flexible blades are attached to the disk. At last, another rigid axisymmetric disk is considered, to represent the axial bearing, which is

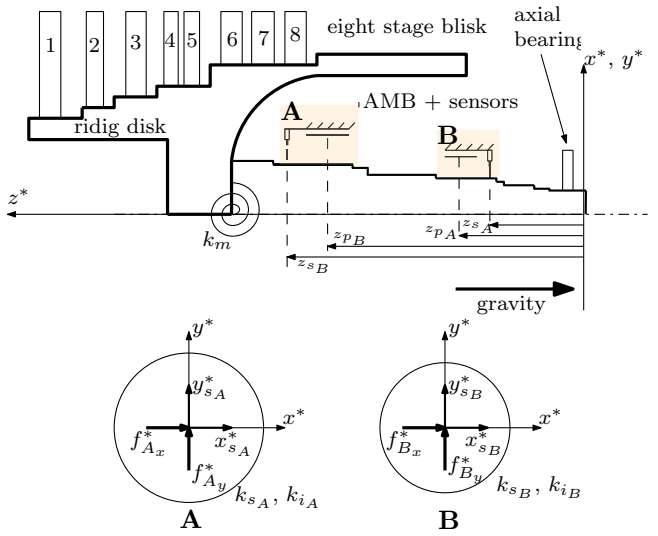

FIGURE 1: MODEL DESCRIPTION: MECHANICAL PARTS AND MAGNETIC BEARINGS POSITIONING

used to levitate the pump when it is set up in vertical position.

The equations of motion are developed in [10] in the rotating frame, based on the works of [15–17]. The phenomenology of flexible parts are described by rotating Euler-Bernoulli beams, their continuous displacements are approximated by Ritz functions and Rayleigh-Ritz method is used for calculating natural frequencies and mode shapes.

The equations of motion for the complete structure are written in Eq. (1). $\mathbf{M}$, $\mathbf{D}$, $\mathbf{K}$, $\mathbf{G}(\Omega)$, $\mathbf{N}(\Omega^2)$ and $\mathbf{K}_{stiff}(\Omega^2)$ are the mass, structural damping, structural stiffness, gyroscopic, spin softening and spin stiffening matrices, respectively.

$$\mathbf{M}\ddot{\boldsymbol{q}} + (\mathbf{D} + \mathbf{G}(\Omega))\boldsymbol{q} + \left(\mathbf{K} + \mathbf{K}_{stiff}(\Omega^2) + \mathbf{N}(\Omega^2)\right)\boldsymbol{q} = \boldsymbol{f} \quad (1)$$

By introducing blades dynamics to the model, the system becomes asymmetric. This is the reason why Eq. (1) is written in the rotating frame R, to avoid time dependent periodic terms in structural matrices [18]. On the other side, magnetic bearings are described in the stationary frame, as shown in the next section. As the control forces are not assumed to be the same on both xz and yz planes, their projection on rotating frame would result in time periodic terms. This problem is treated further in this article as well as the description of how it is introduced in the control loop.

Magnetic Forces

Magnetic bearings dynamics are introduced to the mechanical model as excitation forces in Eq. (1). Their model is developed from the concepts of magnetic circuits and Lorentz forces

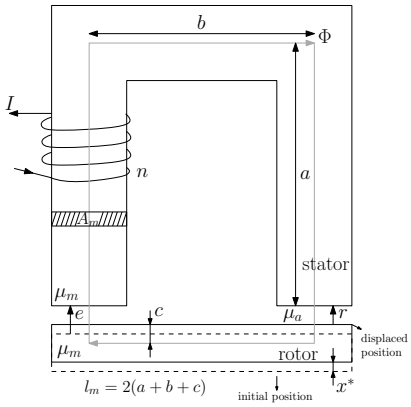

FIGURE 2: MAGNETIC CIRCUIT

[3]. Figure 2 shows a schematic description of such circuits. The magnetic flux Φ that passes by the rotor and stator through a cross section A_m generates the magnetic force F_{mag}. This flux is induced by electric current I passing by n turns of a solenoid. The expression of F_{mag} is given by :

$$F_{mag} = 4A_m n^2 \frac{\mu_0}{\mu_a} \frac{I^2}{\left(\frac{l_m}{\mu_m} + \frac{2r}{\mu_a}\right)^2} \quad (2)$$

where l_m is the mean magnetic flux path length through metallic part, μ_0, μ_a et μ_m are the magnetic permeability at vacuum, air and the magnetic circuit material, respectively. r is the distance between stator and rotor in its displaced position. For further details, see [19].

Equation (2) shows the magnetic force nonlinear dependence on r^2 and I^2. Besides, magnetic forces present a saturation point due to magnets physical properties. Furthermore, F_{mag} and r have the same sign, which makes the magnetic bearings unstable. In our study, the magnetic forces are linearized around an operating point by a first order Taylor expansion of F_{mag}. For that, two variables transformations are performed :

$$r = e + x^*$$
$$I = i_o + i$$

where e is the initial distance from rotor to bearing, x^* is the displacement of the rotor in the stationary frame[1], i_0 is the bias current and i the control current.

This leads to magnetic forces linearized expression:

[1] also valid for y^*

$$F_{mag} = -K_s x^* + K_i i \tag{3}$$

The expression (3) is valid for one direction of one actuator. The rotor is equipped with two sensors and actuators on each xz and yz plane. The integration of this four forces to the mechanical system is proposed in the next section.

Coupling of the Mechanical System and Magnetic Bearings

As described in Fig. 1, two magnetic bearings are mounted on the shaft, defining two control planes (identified by **A** and **B**). For each plane, displacement sensors in x^* and y^* directions are mounted. The forces delivered by the magnetic bearings are noted $\boldsymbol{F}_a^* = \left\{ f_{A_x}^*, f_{B_x}^*, f_{A_y}^*, f_{B_y}^* \right\}^T$, and the displacements measured by the sensors are noted $x_s^* = \left\{ x_{s_A}^*, x_{s_B}^*, y_{s_A}^*, y_{s_B}^* \right\}^T$. As sensors and actuators are not colocalized, displacements of the shaft at sensors and actuators positions are not the same, and for the latter, they are noted as $\boldsymbol{x}_p^* = \left\{ x_{p_A}^*, x_{p_B}^*, y_{p_A}^*, y_{p_B}^* \right\}^T$. The expression of the magnetic forces vector is then :

$$\boldsymbol{F}_a^* = -\mathbf{K}_s x_p^* + \mathbf{K}_i \boldsymbol{i}_a \tag{4}$$

where

$$\mathbf{K}_s = \text{diag}([k_{s_A}, k_{s_B}, k_{s_A}, k_{s_B}])$$

and

$$\mathbf{K}_i = \text{diag}([k_{i_A}, k_{i_B}, k_{i_A}, k_{i_B}])$$

The integration of the expression (4) into the equations of motion (1) needs two major adaptations: (1) forces must be projected on the rotating frame and (2) physical displacements must be written in Rayleigh-Ritz basis. Projection from stationary to rotating frame is made by means of $\mathbf{R}(\Omega t)$ matrix (see Eq. (13) in the appendix A):

$$\boldsymbol{F}_a = \mathbf{R}(\Omega t)\, F_a^* \tag{5}$$
$$x_p = \mathbf{R}(\Omega t)\, x_p^* \tag{6}$$

The relations between physical and generalized coordinates are given by (matrices Θ_s and Θ_p are described in the appendix):

$$\boldsymbol{x}_s = \Theta_s\, q \tag{7}$$
$$\boldsymbol{x}_p = \boldsymbol{\Theta}_p\, q \tag{8}$$

Generalized forces are the result of the derivative of the work with respect to the generalized coordinates [20]. The work of the magnetic forces is defined in the stationary frame as:

$$\delta W_{F_a} = \delta(\mathbf{x}_p^*)^T \boldsymbol{F}_a^* \tag{9}$$

Combining Eq. (4), (8), and (9) and considering that $\mathbf{R}(\Omega t)\mathbf{K}_s\mathbf{R}^T(\Omega t) = \mathbf{K}_s$, the work expression in terms of displacements described in the rotating frame is obtained:

$$W_{F_a} = -\boldsymbol{q}^T \boldsymbol{\Theta}_p^T \mathbf{K}_s \boldsymbol{\Theta}_p \boldsymbol{q} + \boldsymbol{q}^T \boldsymbol{\Theta}_p^T \mathbf{R}^T(\Omega t)\, \mathbf{K}_i \boldsymbol{i}_a \tag{10}$$

The expression of the generalized magnetic forces described in the rotating frame is then:

$$\boldsymbol{F}_a = -\Theta_p^T \mathbf{K}_s \boldsymbol{\Theta}_p q + \Theta_p^T \mathbf{R}^T(\Omega t)\, \mathbf{K}_i i_a \tag{11}$$

Combining Eq. (11) and (1) leads to the expression of the electromechanical system, written in a state-space form in Eq. (12). It is clear from this equation that the dynamic characteristics of the coupled system depends on the control current vector i_a. To stabilize the system and reach good dynamic performances, the control law that defines $\boldsymbol{i}_a$ is described in the next section.

$$\begin{cases} \begin{bmatrix} \boldsymbol{q} \\ \ddot{\boldsymbol{q}} \end{bmatrix} = \mathbf{A} \begin{bmatrix} \boldsymbol{q} \\ \dot{\boldsymbol{q}} \end{bmatrix} + \mathbf{B}\, \mathbf{K}_i \boldsymbol{i}_a \\ \boldsymbol{x}_s = \begin{Bmatrix} x_{s_A} \\ x_{s_B} \\ y_{s_A} \\ y_{s_B} \end{Bmatrix} = \boldsymbol{\Theta}_s \begin{bmatrix} \boldsymbol{q} \\ \dot{\boldsymbol{q}} \end{bmatrix} \end{cases} \tag{12}$$

$$\mathbf{A} = \begin{bmatrix} \mathbf{0} & \mathbf{I} \\ -\mathbf{M}^{-1}\left(\mathbf{K} + \mathbf{K}_{mag} + \mathbf{K}_{stiff} + \mathbf{N}\right) & -\mathbf{M}^{-1}(\mathbf{D} + \mathbf{G}) \end{bmatrix}$$

with $\mathbf{K}_{mag} = \Theta_p^T \mathbf{K}_s \boldsymbol{\Theta}_p$

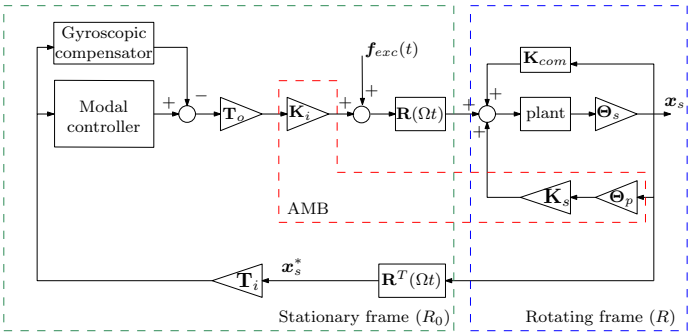

FIGURE 3: CONTROL LOOP

$$\mathbf{B} = \begin{bmatrix} \mathbf{0} \\ \mathbf{M}^{-1}\boldsymbol{\Theta}_p^T\mathbf{R}^T(\Omega t) \end{bmatrix}$$

The complete system has dimension 452, which is a very small model compared to the phenomenology it is able to describe: the overall dynamics of an eight stages flexible bladed rotor with gyroscopic effects, spin softening, blades centrifugal stiffening, and the possibility of including a mistuning pattern, since all of the blades are modeled. This point is very important in industrial design processes, since small models need short computation time to be simulated.

In this section, the equations of the electromechanical coupled system were obtained in state-space form, defining the mechanical system behavior dependence on control currents. In the next section, the control law used to define currents that stabilize the coupled system is presented.

Control law

The control loop strategy used for the simulations are inspired from the work of [21] and is represented in Fig. 3. It consists of decoupled modal controllers acting independently on each rigid body modes. These independent controllers are composed of a PID, as well as second order lag and lead-lag filters that damps the flexible modes. Gyroscopic compensation is implemented in order to minimize variations in plant characteristics and guarantee controller performance for all the spin speed range.

In order to control independently the modes, displacements $\boldsymbol{x}_s$ are expanded on the modal basis, without the magnetic bearings. The dimension of this modal basis defines the number of controllable modes, and is limited by the number of sensors available [22], unless a state observer is implemented. On the other side, modal controller output must be projected to the physical basis, so that AMB forces can be calculated. Such transformations are represented by $\mathbf{T}_i$ and $\mathbf{T}_o$, before and after the modal controller block in Fig. 3.

To define the control law, system is considered axisymmetric: blades flexibility are not taken into account, disk's mass and moment of inertia are increased to integrate blades' influence. In that way, the equations of the coupled system do not present time-periodic terms in both stationary and rotating frames. Thus, stability of the system can be assessed by traditional methods. To do so, only structural matrices corresponding to shaft and disk are included in Eq. (12), and projection to stationary frame is possible thanks to Eq. (14) given in appendix C. Once this control law has proven its performance and stability for the axisymmetric system, it will be tested on the complete mechanical model, including blades flexibility.

The obtained modal controller is composed of independent PID controller combined with lag and lead-lag filters for each controlled mode. PID parameters are tuned to define rigid body modes frequency and damping. Second order filters are tuned to damp flexible modes by shifting the phase at specific frequencies. The following paragraphs focus on the stability analysis of the obtained controller for the axisymmetric system.

RESULTS FOR THE AXISYMMETRIC SYSTEM

This section shows a first step of analysis before considering the complete asymmetric model. The objective is to verify that the closed loop simulations are stable for the axisymmetric system before the integration of blades flexibility, which increases considerably the model's complexity. For the axisymmetric system, the control loop is slightly different from the one described in Fig. 3: plant model is written in the stationary frame, as well as the magnetic bearings forces, so blocks $\mathbf{R}(\Omega t)$ and $\mathbf{R}^T(\Omega t)$ are not necessary. The control loop is implemented in Matlab© using tools from the Control System Toolbox.

For the stability analysis, the closed loop poles were calculated for each spin speed (Ω) and plotted in Fig. 4 and 5. For confidentiality issues, all frequencies in paper are normalized by an arbitrary value ω_{ref}.

Stability Analysis and Influence of the Gyroscopic Compensation

First of all, we focus on the impact of gyroscopic compensation on the system. For that, simulations were done without this control block. Figure 4 shows the closed loop poles evolution for this case. Rigid body modes frequencies are indicated by RB and the shaft flexible modes by S. We notice the gyroscopic effects by the split of the natural frequency evolution in two branches, representing the forward (ascending) and backward (descending) whirling modes. One of the rigid body modes interacts with a controller pole at about 48 % of nominal spin speed (Ω_n). Such interaction creates an unstability on the system, that is observable in Fig. 4b. Indeed, at about 50 % of Ω_n a controller pole

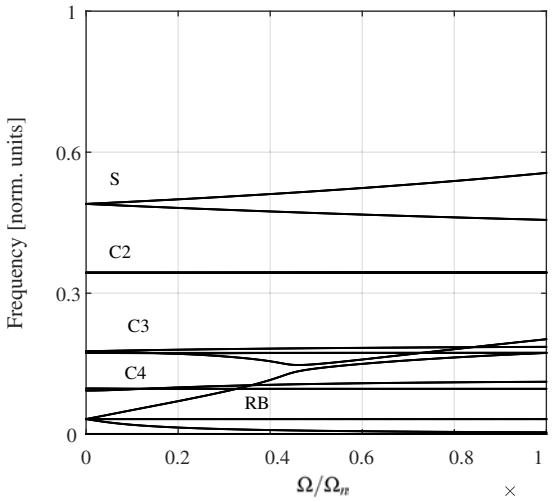

(a) Evolution of the poles norm versus normalized spin speed (Ω/Ω_n)

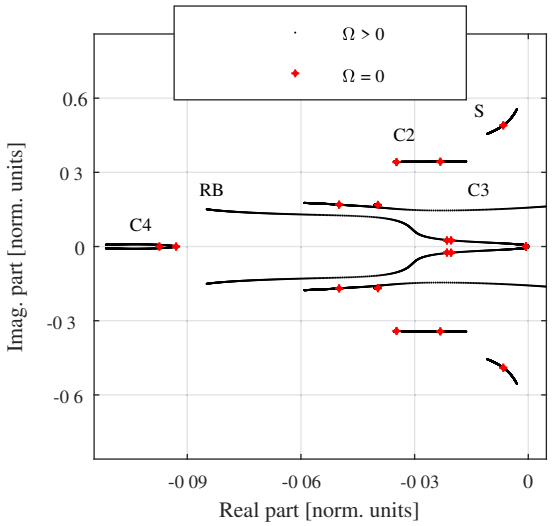

(b) Evolution of the poles versus normalized spin speed (Ω/Ω_n) in complex plane. Real and imaginary parts are normalized by ω_{ref}

FIGURE 4: AXISYMMETRIC SYSTEM POLES WITHOUT GYROSCOPIC COMPENSATION. C: Controller poles, RB: Rigid body modes, S: Flexible shaft modes

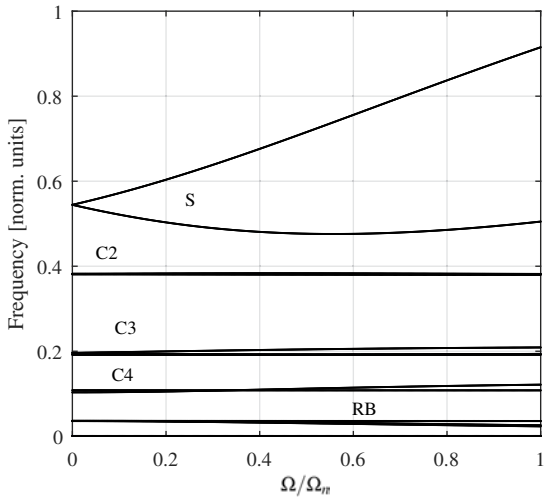

(a) Evolution of the poles norm versus normalized spin speed (Ω/Ω_n)

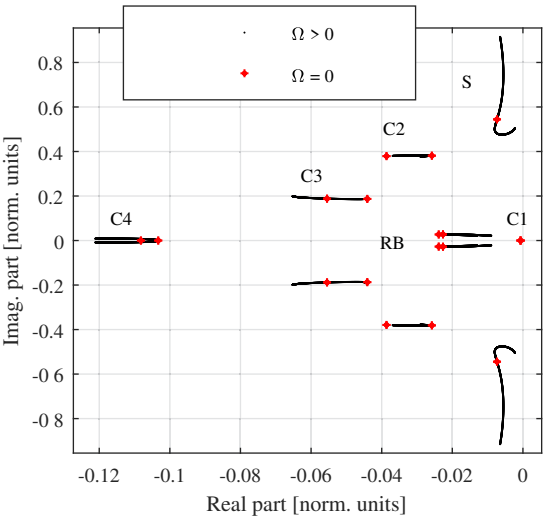

(b) Evolution of the poles versus normalized spin speed (Ω/Ω_n) in complex plane. Real and imaginary parts are normalized by ω_{ref}

FIGURE 5: AXISYMMETRIC SYSTEM POLES WITH GYROSCOPIC COMPENSATION. C: Controller poles, RB: Rigid body modes, S: Flexible shaft modes

is located on the right half of the complex plane. Such results illustrate the fact that spin speed is likely to affect the efficiency of the controller and therefore the closed loop stability.

The results for the gyroscopic compensated case are shown in Fig. 5. It can be noticed in Fig. 5a that controller poles are less sensitive to spin speed. Rigid body modes remains almost constant for all operating speeds. There is no interaction between rigid body modes and controller poles, hence system is stable. To prove stability, Fig. 5b shows the closed loop poles for all spin speeds located on the left half of the complex plane. These results show that gyroscopic compensation is effective to counteract the effects of spin speed on the mechanical behavior of the rotor. Indeed, the natural frequencies stay almost constant along spin speed allowing the controller to be efficient for the whole

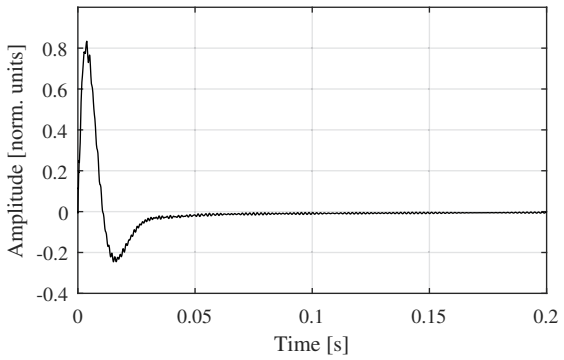

(a) Time Response ($x^*_{s_A}$) - $\Omega = 0$. Amplitudes are normalized by x^*_{ref}

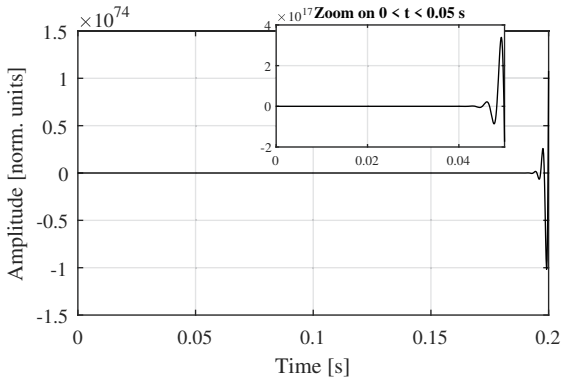

(b) Time Response ($x^*_{s_A}$) - 20% of Ω_n. Amplitudes are normalized by x^*_{ref}

FIGURE 6: IMPULSE RESPONSE OF THE COMPLETE MODEL

operating range.

Comparisons between Fig. 4a and Fig. 5a reveal that the angle between the two flexible shaft modes are considerably larger for the gyroscopic compensated case, yet the expected results would be the opposite. Such effect is a consequence of the modal basis size used for the displacements projection. Since it is only composed by rigid body modes, flexible modes are not controlled but are subject to the controller's action: in this case, controllers increase gyroscopic effects for shaft flexible modes.

With all of these results, the stability of the axisymmetric system for the whole spin speed range is proven. We will now introduce the blades flexibility and evaluate how the closed loop system performances may be affected.

CONTROLLED COMPLETE MODEL SIMULATION

In this section the complete rotating model simulation is presented. Influence of blades flexibility on the closed loop for the rotating model is studied by the response of an impulsive force applied by magnetic bearings. From these results, interaction between blades dynamics and the controller is shown.

Figure 6 presents the time results for (a) the rotor for $\Omega = 0$ and (b) rotating rotor at 20 % of its nominal speed (Ω_n). The plotted displacements correspond to the ones measured by sensor A in the x direction, in the stationary frame. For $\Omega = 0$, time response shows a transient phase that is very quickly damped and the rotor tends to its center position ($x_{s_A} = 0$). However, the rotating system response is divergent, which means that it is unstable for this spin speed. These results does not agree with the stability analysis done with the axisymmetric system shown in Fig. 5, as all of the poles are on the left half complex plane. This behavior indicates that an interaction between the controller poles and the flexible blades modes occurs, which destabilizes the system.

In paper [10], an equivalent flexible model was studied with linear bearings instead of AMB. Results of these analysis are reproduced in Fig. 7 in dotted lines. The axisymmetric system poles evolution are ploted in full lines, as in Fig. 5a. Comparison of these two curves is focused on the region near the normalized frequency of 0.4. There is a superposition of a controller pole, corresponding to a second order filter, with the blades modes for all the speed range. This indicates that there must be an interaction between these two modes, in a similar way than the one observed in Fig. 4a between a controller pole and a rigid body mode. Since stability analysis is not yet carried out for the complete system in rotation, it is not possible to reproduce this interaction. Thus, to sustain this hypothesis, a simulation of the complete AMB suspended system in rotation is carried out, without the 2$^{\text{nd}}$ order filters.

Results of this simulation at 20% of the nominal speed are shown in Fig. 8. The time response is no longer divergent (Fig. 6b). The transient phase is very clear, and the rotor converges to its center of rotation, though more oscillation is observed than for $\Omega = 0$. Figure 8b presents the frequency domain response, normalized by the input force. The typical high level responses at low frequencies are present and at higher frequencies, the peaks corresponding to blades (identified by the letter B) and shaft forward (S-FW) and backward (S-BW) modes are highlighted.

Finally, a comparison between the closed loop system with and without the second order filters at $\Omega = 0$ is shown in Fig. 9. In frequency response (9b), pics corresponding to structural modes are well defined: a high modal density region, corresponding to blades modes has been identified by letter B. The shaft mode was identified by the letter S. Responses without the second order filters have higher amplitude than those with these controller elements, specially at the frequencies near the blades natural frequencies.

These differences are also observed in time domain. In a global view of Fig. 9a, both curves are almost superposed. Indeed, the high amplitude, low frequency response is not affected by the filter since its action is at higher frequencies only. Fo-

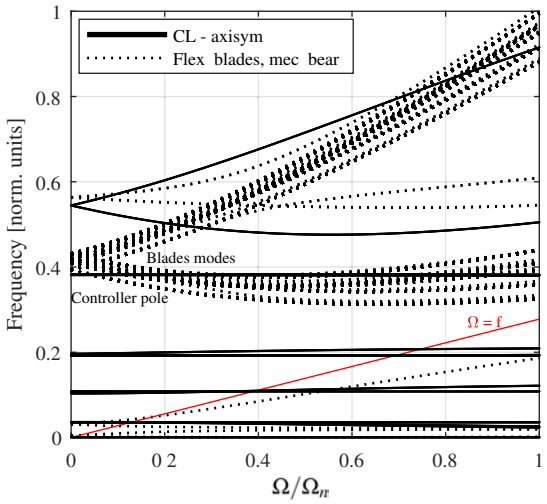

FIGURE 7: COMPARISON OF FULL MODEL ON LINEAR BEARINGS AND AXISYMMETRIC MODEL ON AMB. Frequencies are normalized by ω_{ref}

cusing on the zoom showed in this figure, which includes a late transient phase portion, the amplitudes for the case without the 2nd order filters are greater than those for the case with the second order filters. This indicates that such controller elements are efficient on damping high frequency response corresponding to flexible modes. Since it does not act at low frequencies, frequency response curves are almost identical in this region, as well as the time response.

Those results show that blades flexibility is an important factor to assess the stability of turbomolecular pumps on AMB. Indeed a controller that is stable and well damped for all the spin speed range for the axisymmetric case may not present satisfactory dynamic behavior for the flexible blades case: either unstability is present, or time response is very oscillatory, indicating very small damping for the case without the second order filters.

In real applications, it is important to keep those filters. Besides damping flexible modes, they limit the controller bandwidth, avoiding excitation of high frequency modes that are not taken into account in the controller design. It is then necessary to redesign them in order to avoid the interactions mentioned in the previous paragraphs. To do so, time-periodic systems analysis could be used, as LTI control design theories (classical, optimal or robust control theories, for example) are not sufficient to integrate blades flexibility analysis. Nevertheless, this kind of analyses are not presented in this article as it is outside the scope of our work.

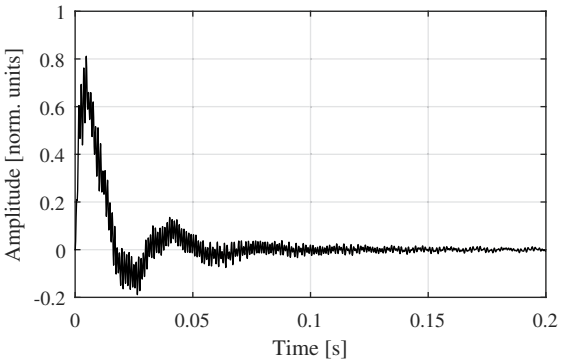

(a) Time Response ($x^*_{s_A}$) - 20% of Ω_n. Amplitudes are normalized by x^*_{ref}

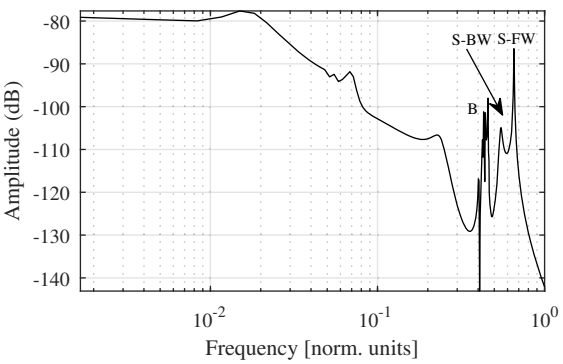

(b) Frequency Response ($x^*_{s_A}/f^*_{A_x}$) - 20% of Ω_n. Amplitudes are normalized by x^*_{ref}

FIGURE 8: IMPULSE RESPONSE OF THE COMPLETE MODEL WITHOUT SECOND ORDER FILTERS. B: Blade modes; S-BW: Shaft backwards whirl mode; S-FW: Shaft forwards whirl mode

CONCLUSIONS AND PERSPECTIVES

This paper describes the simulations of a complete rotating model on controlled active magnetic bearings including shaft and blades flexibility. Response to an impulse excitation is studied. The simulations involves frame changes within the control loop, since magnetic bearings and mechanical parts are not modeled in the same frame. The rotor equations of motion are derived in the rotating frame in order to avoid time-periodic matrices due to blades flexibility. Magnetic bearing forces are defined in the stationary frame, and their projection on the rotating frame is also periodic time dependent.

The developed turbomolecular pump's rotor model has small dimensions, which allows very short calculations for the complete system. In addition, results from simulations of this model on linear mechanical bearings have shown good correlation with experimental data. Thanks to this, tackle the complete

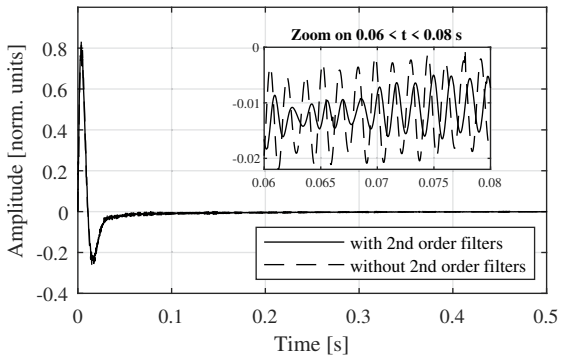

(a) Time Response ($x^*_{s_A}$) - $\Omega = 0$. Amplitudes are normalized by x^*_{ref}

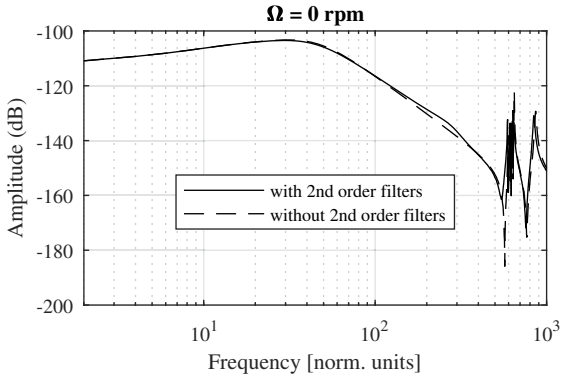

(b) Frequency Response ($x^*_{s_A}/f^*_{A_x}$) - $\Omega = 0$

FIGURE 9: COMPARISON OF FREQUENCY RESPONSES WITH AND WITHOUT 2nd ORDER FILTERS. COMPLETE MODEL. B: Blade modes; S: Shaft modes

closed loop system behavior in the presence of a controller is straightforward. In addition, it can be integrated to the controller design phase. Anticipate the interactions between the controller and all the rotor parts may help in the design to prevent unstabilities.

The results at rest for the complete system have shown stable behavior, and the frequency response reproduces fairly the pics corresponding to structural modes. When the system is in rotation, its response is divergent due to the interaction between blade modes and one pole of the controller that would be responsible for damping the shaft flexible modes. When this element of the controller is taken out of the control loop, the response of the system is very oscillatory, highlighting that the response is weakly damped.

Our simulations underline the impact of blades and shaft flexibility on a classical stable controller (derived from the axisymmetric case). Indeed, the loss of stability of such controller leads to the controller design modification to achieve acceptable performances.

Further work may extend the stability analysis studies for the complete rotating system. To do so, It would be necessary to apply linear time-periodic dependent systems stability analysis methods [11–14]. Such analysis would be of great interest for the controller design as all of the closed loop poles placements would be known.

In parallel, the presented model may be used for blade's mistuning analysis. As all of the blades are modeled, the introduction of a mistuning pattern on it is straightforward. It would then be possible to examine its effects on the stability of the closed loop system, and its influence on the controller's interaction with the blades.

ACKNOWLEDGMENT

The authors thank Pfeiffer Vacuum SAS and its R&D team for their technical and financial support to this work.

REFERENCES

[1] Tamisier, V., Carrère, F., and Font, S., 2002. "Synchronous unbalance cancellation across critical speed using a closed-loop method". In Proceedings of the Eighth International Symposium on Magnetic Bearings, pp. 399–404.

[2] Heldner, M., and Kabelitz, H.-P., 1990. "Reliability of turbomolecular vacuum pumps: A comparison of rolling element and magnetic bearing systems". *Journal of Vacuum Science & Technology A: Vacuum, Surfaces, and Films,* ***8***(3), pp. 2772–2777.

[3] Bleuler, H., Cole, M., Keogh, P., Larsonneur, R., Maslen, E., Okada, Y., Schweitzer, G., Traxler, A., et al., 2009. *Magnetic bearings: theory, design, and application to rotating machinery*. Springer Science & Business Media.

[4] Defoy, B., Alban, T., and Mahfoud, J. "Assessment of the effectiveness of a polar fuzzy approach for the control of centrifugal compressors". *Journal of Dynamic Systems, Measurement, and Control,* ***136***(4), pp. 041004–041004–8.

[5] De Lepine, X., Der Hagopian, J., and Mahfoudh, J., 2006. "Development of a Condensed Reduced Model Based Modal Control Method for Rotors Supported by Active Magnetic Bearings". In The Tenth International Symposium on Magnetic Bearings.

[6] De Miras, J., Join, C., Fliess, M., Riachy, S., and Bonnet, S., 2013. "Active magnetic bearing: A new step for model-free control". In 52nd IEEE Conference on Decision and Control (CDC 2013), pp. 7449–7454.

[7] Han, B., Xue, Q., Liu, X., and Wang, K., 2017. "Multi-objective optimization design of a high-speed pm machine supported by magnetic bearings". *Mechanical Systems and Signal Processing,* ***92***, pp. 349–363.

[8] Sun, X., Su, B., Chen, L., Yang, Z., Xu, X., and Shi, Z., 2017. "Precise control of a four degree-of-freedom permanent magnet biased active magnetic bearing system in a magnetically suspended direct-driven spindle using neural network inverse scheme". *Mechanical Systems and Signal Processing,* ***88***, pp. 36–48.

[9] Dumartineix, C., Thouverez, F., Chouvion, B., and Parent, M.-O., 2018. "An efficient approach for the frequency analysis of non-axisymmetric rotating structures: application to a coupled bladed bi-rotor system". In Proceedings of ASME Turbo Expo 2018: Turbomachinery Technical Conference and Exposition.

[10] Moreira, A. B. B., and Thouverez, F., 2019. "Dynamic modelling and vibration control of a turbomolecular pump with magnetic bearings in the presence of blade flexibility". In *Rotating Machinery, Vibro-Acoustics & Laser Vibrometry, Volume 7*. Springer, pp. 101–110.

[11] Christensen, R. H., and Santos, I., 2005. "Design of active controlled rotor-blade systems based on time-variant modal analysis". *Journal of sound and vibration,* ***280***(3-5), pp. 863–882.

[12] CALICO, R. A., and WIESEL, W. E. "Control of time-periodic systems". pp. 671–676.

[13] Liu, K., 1999. "Extension of modal analysis to linear time-varying systems". *Journal of Sound and Vibration,* ***226***(1), pp. 149–167.

[14] Liu, K., 1997. "Identification of linear time-varying systems". *Journal of Sound and Vibration,* ***206***(4), pp. 487–505.

[15] Parent, M.-O., Thouverez, F., and Chevillot, F., 2014. "Whole engine interaction in a bladed rotor-to-stator contact". In ASME Turbo Expo 2014: Turbine Technical Conference and Exposition, American Society of Mechanical Engineers, pp. V07AT31A003–V07AT31A003.

[16] Gruin, M., Thouverez, F., Blanc, L., and Jean, P., 2011. "Nonlinear dynamics of a bladed dual-shaft". *European Journal of Computational Mechanics/Revue Européenne de Mécanique Numérique,* ***20***(1-4), pp. 207–225.

[17] Lesaffre, N., Sinou, J.-J., and Thouverez, F., 2007. "Contact analysis of a flexible bladed-rotor". *European Journal of Mechanics-A/Solids,* ***26***, pp. 541–557.

[18] Friswell, M. I., Penny, J. E., Garvey, S. D., and Lees, A. W., 2010. *Dynamics of rotating machines*. Cambridge University Press.

[19] Hutterer, M., and Schrödl, M., 2017. "Control of active magnetic bearings in turbomolecular pumps for rotors with low resonance frequencies of the blade wheel". *Lubricants,* ***5***(3), p. 26.

[20] Gmür, T., 1997. *Dynamique des structures: analyse modale numérique*. PPUR presses polytechniques.

[21] Hutterer, M., Hofer, M., and Schrödl, M., 2015. "Decoupled control of an active magnetic bearing system for a high gyroscopic rotor". In Mechatronics (ICM), 2015 IEEE International Conference on, IEEE, pp. 210–215.

[22] Couzon, P.-Y. Contrôle actif neuro-flou de structures : application aux rotors supportés par paliers magnétiques actifs.

Appendix A: Rotation Matrix R

$$\mathbf{R}(\Omega t) = \begin{bmatrix} \cos(\Omega t) & 0 & \sin(\Omega t) & 0 \\ -\sin(\Omega t) & 0 & \cos(\Omega t) & 0 \\ 0 & \cos(\Omega t) & 0 & \sin(\Omega t) \\ 0 & -\sin(\Omega t) & 0 & \cos(\Omega t) \end{bmatrix} \tag{13}$$

Matrix $\mathbf{R}(\Omega t)$ presents the following properties:

$\mathbf{R}^{-1}(\Omega t) = \mathbf{R}^{T}(\Omega t)$
$\mathbf{R}^{-1}(\Omega t)\,\mathbf{R}(\Omega t) = \mathbf{R}^{T}(\Omega t)\,\mathbf{R}(\Omega t) = \mathbf{I}$, where $\mathbf{I}$ is the identity matrix.

Appendix B: Matrices for the Transformation Between Physical and Generalized Coordinates

$$\mathbf{\Theta}_p = \begin{bmatrix} W_1(z_{p_1}) & \dots & W_{m_{tot}}(z_{p_1}) & 0 & \dots & 0 & 0 \cdots 0 \\ W_1(z_{p_2}) & \dots & W_{m_{tot}}(z_{p_2}) & 0 & \dots & 0 & 0 \cdots 0 \\ 0 & \dots & 0 & W_1(z_{p_1}) & \dots & W_{m_{tot}}(z_{p_1}) & 0 \cdots 0 \\ 0 & \dots & 0 & W_1(z_{p_2}) & \dots & W_{m_{tot}}(z_{p_2}) & 0 \cdots 0 \end{bmatrix}$$

$$\Theta_s = \begin{bmatrix} W_1(z_{s_1}) & \dots & W_{m_{tot}}(z_{s_1}) & 0 & \dots & 0 & 0 \cdots 0 \\ W_1(z_{s_2}) & \dots & W_{m_{tot}}(z_{s_2}) & 0 & \dots & 0 & 0 \cdots 0 \\ 0 & \dots & 0 & W_1(z_{s_1}) & \dots & W_{m_{tot}}(z_{s_1}) & 0 \cdots 0 \\ 0 & \dots & 0 & W_1(z_{s_2}) & \dots & W_{m_{tot}}(z_{s_2}) & 0 \cdots 0 \end{bmatrix}$$

In these matrices $W_1 \cdots W_{m_{tot}}$ are Ritz functions that describe the displacements of the shaft; z_{p_1}, z_{p_2}, z_{s_1} and z_{s_2} are the positions of actuators and sensors.

Appendix C: Relations Between Structural Matrices in Stationary and Rotating Frame for the Axisymmetric Case

$$\mathbf{M}^{*} = \mathbf{M} \tag{14a}$$

$$\mathbf{D}^* = \mathbf{D} \tag{14b}$$

$$\mathbf{G}^*(\Omega) = \mathbf{G}(\Omega) + 2\mathbf{M}\boldsymbol{\Omega}^I \tag{14c}$$

$$\mathbf{K}^* = \mathbf{K} \tag{14d}$$

$$\mathbf{N}^*\left(\Omega^2\right) = \mathbf{N}\left(\Omega^2\right) - \Omega^2\mathbf{M} + \mathbf{G}\boldsymbol{\Omega}^I = \mathbf{0} \tag{14e}$$